

5-2016

Physical modeling of vortical cross-step filtration in the oral cavity of American paddlefish (*Polyodon spathula*)

Hannah Brooks
College of William and Mary

Follow this and additional works at: <https://scholarworks.wm.edu/honorsthesis>



Part of the [Aquaculture and Fisheries Commons](#), [Biophysics Commons](#), [Integrative Biology Commons](#), [Marine Biology Commons](#), [Structural Biology Commons](#), and the [Zoology Commons](#)

Recommended Citation

Brooks, Hannah, "Physical modeling of vortical cross-step filtration in the oral cavity of American paddlefish (*Polyodon spathula*)" (2016). *Undergraduate Honors Theses*. Paper 916.
<https://scholarworks.wm.edu/honorsthesis/916>

This Honors Thesis is brought to you for free and open access by the Theses, Dissertations, & Master Projects at W&M ScholarWorks. It has been accepted for inclusion in Undergraduate Honors Theses by an authorized administrator of W&M ScholarWorks. For more information, please contact scholarworks@wm.edu.

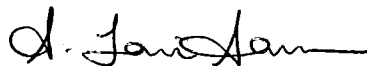
Physical modeling of vortical cross-step filtration in the oral cavity of American paddlefish
(*Polyodon spathula*)

A thesis submitted in partial fulfillment of the requirement
for the degree of Bachelor of Science in Biology from
The College of William and Mary

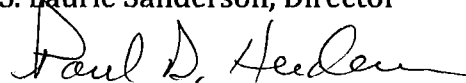
by

Hannah Brooks

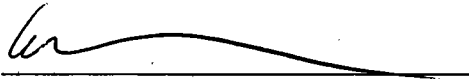
Accepted for Honors



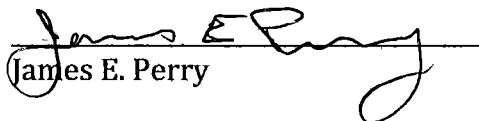
S. Laurie Sanderson, Director



Paul D. Heideman



William Buchser



James E. Perry

Williamsburg, VA
May 4, 2016

Introduction

There are more than 70 species of suspension-feeding fish caught commercially, comprising 25% of the world's fish catch. Additionally, filter-feeding fish play an important ecological role, consuming plankton and improving water quality (Drenner et al., 1987; Lu et al., 2001; Torres et al., 2016; Sanderson et al., 2016) However, the mechanisms that these fish use to retain and transport particles are not well understood. For a long time, it was assumed that filter-feeding fish used dead-end sieve filtration to retain particles. Dead-end sieve filtration occurs when the main flow of water passes perpendicularly through the sieve, and particles larger than the mesh pore size are caught on the mesh surface. However, recently more evidence supports the idea that many fish are using cross-flow filtration.

Cross-flow filtration occurs when the main body of water flows parallel to the filter, carrying most of the particles. As the water flows across the filter, small streams of water escape through the filter. This results in the particles becoming more and more concentrated as they move towards the esophagus, where they will be swallowed (Sanderson et al., 2001; Callan and Sanderson, 2003; Motta et al., 2010; Smith and Sanderson, 2013; Paig-Tran et al., 2013). Many industries utilize this method of filtration (Jaffrin, 2012), but the mesh in the industrial cross-flow filters clogs while the fish filters do not. Therefore, research on fish filtration can help increase the efficiency of industrial filtration. (<http://www.nature.com/nature/journal/v412/n6845/full/412387a0.html>)

A third, more elaborate, filtration mechanism has recently been proposed for North American paddlefish. This method is called vortical cross-step filtration, and utilizes

backward-facing steps to form vortices that transport particles. The vortices clear particles from a large portion of the mesh behind each step, preventing clogging, and transport particles within the slit between backward-facing steps (Sanderson et al., 2016). In paddlefish, thin cartilaginous gill arches form the steps, and the spaces between gill arches form the slits.

In this thesis, the vortices in cross-step filtration are explored within North American paddlefish oral cavities. This thesis is the first effort to video and quantify these vortices in preserved paddlefish. North American paddlefish, *Polyodon spathula*, are suspension-feeding fish that live in the Mississippi water basin. While the paddlefish used in this thesis are small, paddlefish can grow up to two meters long. They are found in deeper sections of the river, filter-feeding at the bottom. When it first hatches, the paddlefish hunts and catches plankton. However, as it grows it switches to a filter-feeding lifestyle (Bemis et al., 1997; Jennings and Zigler, 2009). There is only one other extant species of paddlefish, the Chinese paddlefish (*Psephurus gladius*), and the paddlefish's closest relative is the sturgeon. Currently, the North American paddlefish is listed as vulnerable on the IUCN redlist because of anthropogenic impacts and habitat destruction (Grady, 2004).

Filter-feeding fish, in general, feed on 5 – 3000 μm zooplankton and phytoplankton in the water column (Drenner et al., 1984; Smith and Sanderson, 2013; Zhu et al., 2014). Paddlefish feed on particles as small as 0.10 mm, and are non-selective feeders (Rosen and Hales, 1981). The structure of the paddlefish's mouth enables it to capture small particles. Five cartilaginous gill arches extend in the anterior-posterior direction within the paddlefish mouth. Each arch has a ceratobranchial along the oral floor and arches 1

through 4 have an epibranchial along the oral roof. These gill arches are compressed laterally, with a cross section of only 1 – 2 mm in juvenile paddlefish used for this study. Long, thin, ossified gill rakers are attached at the bottom of both sides of these gill arches. These gill rakers are numerous and densely packed (Grande and Bemis, 1991). While paddlefish are ram ventilating, they retract the gill rakers so that they lie flush with the wall of the gill arches. They then swim through the water with their mouths open letting water flow over their gill filaments (Burggren and Bemis, 1992). When the paddlefish switches to ram suspension feeding, it moves the gill rakers so that they lie across the opening between gill arches. These rakers can be as little as 0.04 mm apart at their base near the gill arch (Rosen and Hales, 1981). Vortices form behind the gill arches, transporting particles along the gill arch (Sanderson et al., 2016). Additionally, as the paddlefish swims, it undulates back and forth. This movement could help the paddlefish detect plankton using electrosensory ampullae in its rostrum (Wilkins et al., 1997; Greenwood et al., 2000; Wojtenek et al., 2001). However, this yawing movement could also help the paddlefish move particles in its mouth.

The structure of the paddlefish filtration device is the reason they were chosen for this thesis. The wide oral gape and widely spaced gill arches allow for easy visualization of the flow patterns behind each arch. Additionally, the paddlefish is unique in its placement of the gill rakers at the lateral edge of the arch. Most other filter-feeding fish have gill rakers at the medial edge of their gill arches, with the exception of the basking shark (Sims, 2008). The first main objective of this thesis was to quantify the arch angles and angle of yaw for the paddlefish. The second main objective of this thesis was to study and quantify the vortices formed behind the arches in three different preserved paddlefish specimens.

The third main objective was to study the effect of changing arch angle on vortices formed in conical cross-step 3D models. Finally, the data for the models and paddlefish were compared.

Materials and methods

Paddlefish branchial arch angles

Three juvenile paddlefish (small: 36.6 cm total length (TL) and 19.8 eye-to-fork length (EFL), medium: 39.6 cm TL and 22.6 cm EFL, and large: 50.5 cm TL and 29.0 EFL) were obtained on ice within 24 hours of death from an aquaculture facility in Ohio, Big Fish Farms (William and Mary Institutional Animal Care and Use Committee approval 07/30/14; Virginia Department of Game and Inland Fisheries approval 07/24/14). The fish were labeled small, medium, and large according to their relative sizes. In preparation for preservation in formalin, gauze sponges (5 cm X 5 cm, Dukal 2128) were rolled and placed between the gill arches to simulate suspension-feeding position (Sanderson et al., 1994). Larger gauze sponges (10 cm X 10 cm, Dynarex) were used to maintain the oral cavity in an expanded position. After two weeks in 10% buffered formalin, the specimens were transferred to a 75% ethanol solution.

To trace the angles at which the branchial arches were arranged along the midline of the oral cavity roof and floor in the preserved paddlefish, a fine point permanent marker and acetate sheets were used. A piece of acetate was cut to fit snugly into the upper or lower half of the paddlefish oral cavity. The marker was used to trace over the medial edge of each infrapharyngobranchial and epibranchial in the oral cavity roof, as well as each

ceratobranchial, hypobranchial, and basibranchial in the oral cavity floor (Figure 1). The acetate sheets were then removed from the oral cavity for analysis.

The infrapharyngobranchials in the roof, as well as the basibranchials in the floor, form a V-shape along the midline of the roof or floor, with the point of the "V" facing the posterior oral cavity (Figure 1). Therefore, a line was drawn along the straightest region of each epibranchial and each ceratobranchial, and each line was extended to meet the "V" formed by the infrapharyngobranchials or the basibranchials. The angle at which each epibranchial or ceratobranchial intersected this "V" was quantified using a protractor (Figure 1). For each branchial arch in each paddlefish, the angles from the right and left sides of the oral cavity were averaged together (Table 1).

Area of paddlefish gill slits and oral gape

The area of the gill slits (the openings from which water exits between the branchial arches) was obtained by tracing the medial edges of the branchial arches and basibranchials onto a clear vinyl sheet (20 gauge) as described for the paddlefish branchial arches above (Figure 2). A photograph of each tracing with a millimeter ruler was analyzed in ImageJ 1.49 to obtain the area of each gill slit individually.

To measure oral gape area, each paddlefish was photographed in anterior view with a millimeter ruler next to the eye at the corner of the gape for scale (Figure 3). The paddlefish was oriented so that the rostrum did not obscure any portion of the oral gape. A drawing tool in ImageJ 1.49 was used to trace the perimeter of the open mouth, and the magic wand tool was used to select the oral gape area. For each paddlefish, the oral gape area was compared to the area of the gill slits.

Aspect ratio of paddlefish branchial arches

Calipers were used inside the preserved paddlefish to obtain the measurements needed to calculate the aspect ratio. Two measurements were taken in the region of the branchial arch where the vortices had been recorded: (1) the width of the gill slit between ceratobranchial one and ceratobranchial two and (2) the height of the first ceratobranchial. These measurements were obtained in order to calculate the aspect ratio for each paddlefish. This ratio describes the gap between the branchial arches (w) related to the height (h) of the branchial arch, and is given by the following equation:

$$\textit{Aspect ratio} = \frac{w}{h}$$

Paddlefish vortex experiments

During feeding in paddlefish, the gill rakers abduct to cover the floor of the gill slits between arches. During ram ventilation and after death, the gill rakers adduct passively to lie vertically against the branchial arches. Since the gill rakers are essential for paddlefish filter feeding, it was necessary to simulate these rakers using a stainless steel mesh (104 μm pore size, Ted Pella Inc.). To prepare the mesh, tracings of the gill slits were obtained as described above for the area of the paddlefish gill slits. The tracing for each gill slit was used as a template when cutting the stainless steel mesh to the correct size and shape. Individual paddlefish varied slightly in the shape of the mesh insert for the gill slit, but the overall shape was the same in all three fish.

Another modification was made to two of the paddlefish: the largest and the medium-sized ones. The mouths of these two paddlefish were not fully open when they

were preserved. In the flow tank, a loop of monofilament was used to pull down the lower jaw of each paddlefish. A length of monofilament was threaded around two spots on the lower jaw, leaving two ends trailing. These ends were tied together to create a loop. The end of this loop was attached to a hook on a suction cup. The suction cup could be positioned on the floor of the flow tank while the paddlefish was positioned inside the tank. This enabled the lower jaw to be abducted further.

Each of the three paddlefish was positioned individually in the center of a recirculating flow tank (18 cm X 18 cm X 90 cm working area, 100 liter total volume). The paddlefish could be oriented so that the rostrum was pointed directly parallel to the oncoming flow or at an angle to the right or left of the oncoming flow. An overhead clamp held the paddlefish by its lower abdomen posterior to the pectoral fins and the operculum.

To visualize the vortices, an infusion needle (25G x 3/4") was inserted through the first branchial arch from a downstream location that was ventral and exterior to the fish oral cavity. The needle was inserted at approximately the junction between the ceratobranchial and the hypobranchial. The needle tip was flush with the posterior wall of the first ceratobranchial and was pointed into the gill slit between the first and second arches. This minimized the needle's effect on the flow patterns between the arches. A syringe with rhodamine water-tracing dye (Cole Parmer) was attached to the infusion needle exterior of the fish, downstream and ventral from the oral cavity. The dye was released from the tip of the infusion needle into the gill slit while water was flowing through the paddlefish oral cavity, allowing visualization and recording of the flow patterns between the arches (120 frames per second, iPhone 5S). Following each recording of the flow patterns, while the camera was still recording from the same position, a millimeter

ruler was placed along the arch of the paddlefish in the location of the flow patterns to provide a scale for analysis. The speed of the flow tank was $18.9 \pm 0.2 \text{ cm s}^{-1}$ for all paddlefish experiments, which is at the low end of the range reported for swimming speeds in live paddlefish of approximately the same body length (Sanderson et al., 1994).

The videos of the vortices were analyzed using iMovie '11 (version 9.0.4). Five vortices were analyzed for each of the three paddlefish. Each clip was paused when the vortex had completed the maximum number of full 360° rotations observable in the camera field of view. The number of frames needed for the vortex to complete these full rotations was converted to the time elapsed. Images of the vortex and the millimeter ruler along the branchial arch were analyzed in ImageJ 1.49 to obtain the vortex diameter and the distance traveled by the vortex along its axis within the gill slit. These values were used to calculate the angular speed, linear speed, rotations per minute, speed of the vortex as it traveled along its axis down the gill slit, and circumference of each of the vortices in Excel (version 14.6.1).

Frames were converted to time (t , in s) by dividing the number of frames counted for the maximum number of rotations R that the vortex completed by the number of frames in one second, 120.

$$\frac{\# \text{ frames for } R \text{ rotations}}{120 \text{ frames s}^{-1}} = t$$

Angular speed (ω , in radians s^{-1}) was calculated by dividing the number of rotations (R , in radians) by the amount of time (t , in s) that it took to complete that number of rotations.

$R \text{ rotations} \times 2\pi \text{ radians per rotation} = R(2\pi) \text{ radians}$

$$\omega = \frac{R(2\pi)}{t}$$

Linear speed (V , in cm s^{-1}) was calculated by multiplying the angular speed (ω , in radians s^{-1}) by the radius of the vortex (r , in cm).

$$V = \omega r$$

Rotational speed (S , in rotations s^{-1}) was calculated by dividing the number of rotations the vortex completed (R) by the amount of time it took to complete those turns (t , in s).

$$S = \frac{R}{t}$$

The vortex speed along its axis as it moved down the gill slit (A , in cm s^{-1}) was also calculated by dividing the distance traveled by the vortex during R rotations (d) by the time it took to travel that distance (t).

$$A = \frac{d}{t}$$

Circumference was calculated by multiplying the radius (r , in cm) by 2π .

$$C = 2\pi r$$

3D model vortex experiments

Vortices in three different physical models were also analyzed. The models were created using SketchUp Pro 2014 (Trimble Navigation), and 3D printed in white nylon plastic (fine polyamide PA 2200, Shapeways). These models had 5 solid ribs separating 5 open slits to simulate the branchial arches and the gill slits between arches (Figure 4). The most anterior solid rib corresponded to the lower and upper jaws, including the most anterior portion of the oral roof. Ribs 2 through 5 of the model corresponded to branchial arches 1-4. The solid end of the cone represented the fifth branchial arch and the esophagus. Each of the three types of model was designed with a specific branchial arch angle: the first had all arches at a 90° angle with respect to the midline of the model roof and floor, the second had all arches at a 55° angle, and the third had all arches at a 110° angle. These angles were chosen because they allowed enough exit area for the incoming water. The slits in models with smaller angles did not provide wide enough openings for all the water entering the model to exit, creating resistance in the models. Additionally, the significant difference between these three angles ensured that if a change in angle affected the vortices, it would be observed.

In the 90° model, the height of the arches was almost equal to the width of the gill slits, with an aspect ratio (wh^{-1}) ranging from 0.9 to 1.6. At the roof of the model, the height of the arches was 3.7 mm. This height increased gradually towards the floor of the model,

where the height of the arches was 6.7mm. The slit width ranged from 6.1-6.9mm (Sanderson et al., 2016).

In paddlefish, the gill rakers are ossified structures attached to all lateral margins of the branchial arches. A nylon mesh (140 μ m pore size, 55% open area, Component Supply Co.) was glued on the exterior of the model to simulate the gill rakers. The total open pore area of the models was 160% of the gape, which allowed water to enter the model without substantial resistance.

Each model was positioned in the center of the flow tank parallel to the oncoming flow so that water entered through the open gape of the model and exited through the mesh covering the slits between the simulated branchial arches. The models were held in place using a wooden sting that attached to the closed posterior of the model. A plastic skirt was attached to the outside of the model to simulate the operculum of the paddlefish. A polyethylene cannula (1.14 mm I.D., 1.57 mm O.D., Intramedic PE-160) attached to a syringe was inserted into a 1.59 mm hole drilled through the solid midline at the top of the model, and positioned so that the tip of the cannula was flush against the top wall inside of the second slit. Rhodamine dye was released into the slits between the ribs of the model to visualize and record the vortices (120 frames per second, iPhone 5S). Each of the models had a millimeter scale on an acetate sheet glued along the exterior of the rib that was immediately anterior to the slit in which the vortices were recorded. The speed of the flow tank was maintained at $18.4 \pm 0.4 \text{ cm s}^{-1}$.

Five vortices were analyzed in the second slit on the right side for each model corresponding to the gill slit between the first and second ceratobranchials in the preserved paddlefish. The same parameters that were calculated or measured for the

paddlefish were also obtained for the models. Time, angular speed, linear speed, speed of the vortex along its axis as it moved down the gill slit, rotational speed, and circumference were calculated using the same equations as listed above for the paddlefish vortices. The analyses were conducted using iMovie '11 (version 9.0.4).

Flow speed experiments

Three techniques were used to measure the speed of the water inside the flow tank. A micro-thermistor flow probe was the only technique that was used to measure the flow inside the paddlefish and the 3D models. The micro-thermistor flow probe quantifies flow using a glass bead thermistor (1.09 mm diameter, 112-101BAJ-01, Fenwal Electronics) that is heated by an electronic circuit. The rate at which heat is stripped from the bead by the flow was used to quantify the flow speed. The flow probe was connected to a circuit modified from LaBarbera and Vogel 1976 (Smith and Sanderson, 2008) and the flow speeds were recorded using a Sonometrics TRX-4 A/D convertor, which sampled the output of the circuit at 200Hz. The probe was threaded through a polyethylene cannula (1.57 mm I.D., 2.08 mm O.D., Intramedic PE-205) for stabilization and placement. Only the glass bead and a short length of wire protruded from the cannula. A second wire with a rod and larger glass bead attached to it was placed in the water as a reference probe downstream from the paddlefish or the model, to ensure that the flow speed reading was not influenced by the temperature of the water.

The cannula with the thermistor flow probe was positioned in different locations exterior and interior of the paddlefish oral cavity to record the speed of the water: (1) 3 cm anterior of the rostrum, (2) directly anterior to the gape at the height of the first

ceratobranchial, and (3) inside the oral cavity directly dorsal to the first ceratobranchial, above the insertion site of the infusion needle. These flow speed measurements were obtained at the conclusion of each paddlefish vortex experiment, prior to moving the paddlefish or the infusion needle.

To measure flow speed in the 90° model, the cannula was inserted into a hole (2.38 mm diameter) drilled in the top midline of the model near the slit between rib two and rib three. This second slit corresponded to the gill slit between ceratobranchial one and ceratobranchial two in the preserved paddlefish. The tip of the cannula was placed flush to the interior wall of the models to ensure that it did not generate a wake. The flow was also recorded 3 cm anterior to the model gape.

A second method was also used to find the flow speed of the water in the flow tank. The movement of a stream of rhodamine dye inside the flow tank was recorded (120 frames per second, iPhone 5S). The video was then analyzed to find the speed that the dye was traveling.

The third method used to measure the flow speed inside the tank was a Geopacks MFP51 flowmeter. The propeller rotates a certain number of times per minute depending on the flow speed and the output is calibrated by the manufacturer to provide speed in cm s^{-1} . This method could not be used to measure flow speed within the paddlefish because the propeller was too large.

Degree of paddlefish yaw

Videos (30 frames s^{-1} , Panasonic WV-2170) taken from directly overhead of paddlefish (36 cm to 45 cm total length, 22 cm to 29 cm eye-to-fork length, Sanderson et al.

1994) swimming in a circular tank (1.2 m diameter X 0.2 m deep) were analyzed to measure the angle at which the paddlefish rostrum yaws to the left and right as they filter fed. A large screen computer (iMac, 27 inch diagonal) in the media center at the College of William & Mary was used to analyze the videos.

A clip was found from the videos in which each paddlefish was swimming in a straight line with no interference. The video was paused and a clear acetate sheet was taped onto the screen. On the sheet, a line was drawn in red permanent marker to indicate the overall direction that the paddlefish was swimming. The clip was then advanced frame by frame, and the paddlefish rostrum and body were traced when the paddlefish had turned completely right or left. The sheet was then removed from the monitor, and a line was drawn from the tip of the paddlefish rostrum to the middle of the traced paddlefish, where the swimming trajectory line intersected with the base of the paddlefish's head (directly posterior to the operculum but anterior to the origin of the pectoral fins). The angle created by the swimming trajectory line and the line through the paddlefish rostrum was measured. Three yaws (the complete oscillation of the paddlefish to either the right or left) were recorded per pass (each time that the paddlefish swam in a straight line with no interference), and three passes were analyzed per fish. There were four fish available to record. One had a short nose (SN), one was small (LG), one was larger and pale (PG), and the last was dark and large (DG).

Statistical Analysis

JMP 12 Mac (SAS Institute Inc.) was used for all statistical tests with a significance level of $p < 0.05$. Levene's tests for homogeneity of variance were performed. To compare

the revolutions per minute, linear speed, diameter, and speed along the axis in the gill slit for vortices in the three 3D models, one-way ANOVAs were used. The same statistical tests were used to compare the same values between the vortices in the three different preserved paddlefish. When the one-way ANOVAs indicated significant differences, Tukey's honest significant difference *post-hoc* test was performed.

Results

Paddlefish branchial arch angles

For the three paddlefish that had been preserved in suspension-feeding position, the mean angle between the straightest section of the lower jaw and the extended basibranchials was 41.9°. The corresponding mean angle between the straightest section of the anterior wall of the first gill slit on the oral cavity roof and the midline of the oral cavity roof was 46.4°. The mean angles between ceratobranchials 1-4 and the basibranchials ranged from 26.1-15.0°, while the mean angles between epibranchials 1-4 and the midline of the oral cavity roof ranged from 41.4-18.3° (Table 1).

The branchial arch angles were consistently larger at the anterior of the paddlefish oral cavity and decreased with each successive arch. However, from anterior to posterior, the ceratobranchial angles decreased more rapidly than the epibranchial angles (Table 1).

Area of paddlefish gill slits and oral gape

The gap between the suspensorium and the first branchial arch was labeled as gill slit 1. The gill slit areas decreased steadily from anterior to posterior (Table 2). As the fifth

branchial arch lacks epibranchials, the most posterior gill slit was restricted to the gap between the ceratobranchials of the fourth and fifth branchial arches. Therefore, the area of gill slit 5 was substantially smaller than the areas of the other gill slits.

For the three paddlefish specimens preserved in suspension-feeding position, the total gill slit area ranged from 145.5 % – 437.7 % of the open gape area (Table 2).

Aspect ratio

The groove aspect ratio is the width of the gill slit divided by the height of the gill slit (wh^{-1}). The groove aspect ratios of the three paddlefish ranged from 0.9 – 1.6. The large paddlefish had the largest aspect ratio (Table 3).

Paddlefish vortex experiments

The variances were not significantly different among the three data sets ($p > 0.05$, Levene's test for homogeneity of variance). The average linear speeds of the vortices varied less between paddlefish (Table 4, Figure 5, $p = 0.06$, one-way ANOVA, $n = 5$) than did the average rotational speeds ($p < 0.0001$). The vortices of the large paddlefish had the lowest linear speed and rotational speed. The small paddlefish had the highest average rotational speed compared to the rotational speeds in the medium and large paddlefish vortices ($p < 0.0001$, Tukey HSD *post-hoc* test), and the highest average linear speed.

The average vortex diameters for the three preserved paddlefish were not significantly different ($p = 0.06$, one-way ANOVA, $n = 5$). The small paddlefish had the smallest diameter of 0.19 cm, the medium paddlefish had the largest value of 0.26 cm, and the large paddlefish had an intermediate value of 0.23 cm.

The vortices traveled at different speeds along their axis in the gill slit ($p = 0.0005$). The vortices in the large paddlefish traveled at significantly greater speeds along their axis in the gill slit than the vortices in the medium paddlefish and the small paddlefish ($p = 0.0003$, and $p = 0.025$ respectively, Tukey HSD *post-hoc* test).

3D model vortex experiments

The variances were not significantly different among the three data sets ($p > 0.05$, Levene's test for homogeneity of variance). The rotational speeds of the vortices in the three models varied significantly ($p < 0.0001$, one-way ANOVA, $n = 5$). Of the three models (90° , 55° , and 110°) the 110° model vortices had the fastest average rotational speed, 943.4 rotations min^{-1} , compared to the 55° model and 90° model (Table 5, Figure 6, $p < 0.0001$ and $p = 0.0008$ respectively, Tukey HSD *post-hoc* test). The 55° model vortices had the slowest average rotational speed, 535.8 rotations min^{-1} . The linear speeds of the vortices in the three models varied significantly ($p = 0.0002$). The 55° model vortices had the fastest average linear speed, 5.8 cms^{-1} , compared to the 90° and 110° models ($p = 0.0002$ and $p = 0.04$ respectively, Tukey HSD *post-hoc* test), and the 90° model vortices had the slowest average linear speed, 2.9 cms^{-1} , compared to the 55° and 110° models ($p = 0.0002$, and 0.02 respectively).

The diameters of the vortices in the three models varied significantly (Table 5, $p < 0.0001$). The 90° model vortices had the same diameter as the 110° model, 0.09 cm, but the 55° model vortices had a wider diameter of 0.21 cm ($p < 0.0001$, Tukey HSD *post-hoc* test). The speed of the vortices along their axis in the slits varied significantly between the

models ($p = 0.001$). The 110° model vortices traveled at a greater speed compared to the vortices in the 55° and 90° models ($p = 0.001$, Tukey HSD *post-hoc* test).

Flow speed experiments

The flow speed 3 cm anterior of the rostrum was the same for the medium and large paddlefish, 12.4 cm s^{-1} (Table 6). The flow speed in front of the small paddlefish's rostrum was faster, 13.2 cm s^{-1} . The flow speed directly anterior to the oral gape at the height of the first ceratobranchial ranged from 9.7 cm s^{-1} to 11.8 cm s^{-1} . The flow speed directly dorsal to the first ceratobranchial, above the insertion site of the infusion needle ranged from 7.9 cm s^{-1} to 11.1 cm s^{-1} , and slowed down marginally in all three paddlefish compared to the flow speed directly anterior to the oral gape at the height of the first ceratobranchial. The mean impeller speed for all three experiments was $18.9 \pm 0.2 \text{ cm s}^{-1}$ ($n = 3$).

Degree of paddlefish yaw

The yaw angle of the rostrum that corresponded to oscillation of the tail ranged from 3.7° to 5.7° for the four paddlefish (Figure 7).

Discussion

Paddlefish branchial arch angles

The angles at which the branchial arches intersected the infrapharyngobranchials in the oral roof and the basibranchials in the oral floor became progressively smaller from branchial arch 1 in the anterior of the oral cavity to branchial arch 4 (Table 1). None of the

arch angles were as large as the angles of the 3D models used in the experiments in this thesis. Epibranchial 1, with an average angle of 46.4° came closest to the 55° model. However, vortices were not analyzed behind this region of the arch in the preserved paddlefish. While we experimented with turning the paddlefish upside down to analyze the vortices downstream from the arches on the roof of the paddlefish oral cavity, they could not be reliably recorded and analyzed.

The largest ceratobranchial angle measured on the oral floor was only 26.1° , less than half the smallest angle of the 3D models. This difference in angles could affect the vortex speed and shape. When analyzing the 3D models in this thesis, the different angles (55° , 90° , and 110°) caused changes in the shape and speed of the vortices. A previous study used plastic soda bottles as models to analyze the differences between filtration with gill slit angles of 90° and 55° , and $1000\ \mu\text{m}$ mesh pore size (Paig-Tran et al., 2011). These models are different from the 3D models this thesis used in that there is a much steeper and faster decrease in width at the back of the model. Their models are more cylindrical, while ours are conical. This changes the flow of the water as it enters each gill slit. In our models, the water changes angle along the solid wall on the inside of the model before entering the gill slit. In their models, the water remains at the same angle and flow speed until it reaches a gill slit. The change in flow angle in our models could result in faster flow speed, and therefore faster flow speed as the water enters the gill slit (Cheer et al., 2001). Additionally, our models have deeper gill slits, creating vortices. The addition of the steps leads to a new kind of filtration: cross-step filtration (Sanderson et al., 2016). Their gill slits are most likely not utilizing vortices because the bottle models have thin walls. These thin

walls do not allow the model to have deep steps, which prevents the formation of large vortices.

Paig-Tran et al. (2011) found that the two models demonstrated different particle retention efficiencies and particle size retention. The 55° model captured smaller particles (< 50 µm) than those retained by the 90° model. The ability of the models to capture particles smaller than the mesh is indicative of cross-flow filtration because a dead-end sieve is only able to capture particles that are larger than the mesh pore size. However, they found that the 55° model was less efficient than the 90° model (Paig-Tran et al., 2011). This may be because their model had a more cylindrical shape than the models used in this thesis, and therefore had different filtration qualities. Regardless, the shift in angle impacted the filtration device, supporting the idea that gill slit angle plays an important role in filtration.

A shift from 90° to 55° has also been shown to cause an increase in volume flow rate through the gill slits and the velocity of flow exiting from the gill slits using a computational model (Cheer et al., 2001). Therefore, a change in angle may affect not only the vortices behind a branchial arch, but also the overall flow rates into and out of the gill slit. The difference in flow speed, flow shape, and branchial arch angle could affect particle retention and transportation by the vortices. Faster flow could affect the flow shape by resulting in a greater rate of shear in the vortices, which could cause the flow to become more turbulent. Another study, which analyzed the particle retention capabilities of 3D models identical to the ones used in this study, found that the three models were able to retain particles equally well (Sanderson et. al., 2016). Therefore, it is possible that

differences among arch angles do not affect the particle retention capabilities of the paddlefish.

We used ceratobranchial 1, the ceratobranchial with the largest angle of 26.1° , to analyze paddlefish vortices. However, the relationship between the cohesiveness of the vortex and the ability of the vortex to retain and transport particles is not known. Future studies could analyze the effect of decreasing arch angle on ability to retain particles. Since the angles of the paddlefish branchial arches change drastically with each successive arch, this may impact the effectiveness of particle retention and transport by the branchial arches.

The paddlefish were preserved in what we assessed as suspension-feeding position based on photographs, videotapes, and personal observations of suspension-feeding paddlefish. However the exact angles of the branchial arches during feeding change with abduction and adduction of the mandible and hyoid, which has not been quantified. Therefore, future studies should analyze the amount of abduction the paddlefish arches achieve during feeding. This will help with the formation of more accurate models and arch angle approximations.

Paddlefish vortex experiments and 3D model vortex experiments

The vortices in cross-step filtration function more like a cross-flow filter than a dead-end sieve filter. The main bulk of water flows parallel to the filter, scouring particles away from the filter. The effectiveness of these vortices may be impacted by their speed and size, which are in turn influenced by the branchial arch angle and the angle at which the water flows over the vortex.

This thesis is the first effort to video and quantify vortices within a fish oral cavity. Sanderson et al. (2016) demonstrated that vortices could be visualized in the oral cavity of preserved paddlefish, and that these vortices can retain and move particles. The vortices were observed scouring the mesh, and moving the particles so that they aggregated on mesh downstream from the arch. The vortices in the 3D models functioned in the same way, clearing particles from the center of the mesh covering the slit between each pair of ribs and moving the particles towards the mesh downstream from each rib (Sanderson et al., 2016). While this validates the use of the 3D models as a comparison with the paddlefish vortices, it is still not completely accurate to the way paddlefish arches perform in reality. In videos available on the web with views into paddlefish oral cavities while the fish are feeding, no aggregates of particles are observed along the gill rakers covering the slit between branchial arches. Although large regions of the gill slits cannot be observed in videotapes and photographs of feeding paddlefish, the lack of aggregates is noticeable when compared to the models used in this thesis. The 3D models used in this thesis successfully transport particles, but still trap them on the mesh. This suggests that processes in addition to vortices may occur inside the paddlefish mouth to transport particles to the posterior of the oral cavity.

Sanderson et al. (2016) were able to manipulate the vortices in the 3D models so that they transported particles along the slots between the arches to the floor of the model, preventing particles from aggregating at the downstream margins of the arch. Therefore, it is feasible that particles could be transported in the vortex to the joints between the ceratobranchials and the epibranchials. For example, menhaden may be using this method to retain particles. Particles retained by menhaden gill rakers have been hypothesized to

move posteriorly along the branchial arch axis toward the ceratobranchial-epibranchial corner, and then toward the esophagus (Friedland, 1985). From this corner, a different flow pattern may be picking up the particles and transporting them to the back of the mouth. Another possibility is that the particles are caught in mucus within the vortex, and then transported to the back of the mouth. Suspension feeding tilapia have been observed to use mucus entrapment to catch small particles, such as phytoplankton, and transport them posteriorly (Sanderson et al., 1996). However, some species of tilapia, such as *Oreochromis aureus*, rely only on cross-flow filtration, and do not utilize mucus to trap particles (Smith and Sanderson, 2007). Therefore, paddlefish could be using mucus to trap particles, or could be relying only on vortices to transport particles. To test this experimentally, an endoscope could be inserted into the paddlefish mouth to observe the particle movement. Regardless, the paddlefish's ability to utilize vortices could explain how they may be capturing and eating particles smaller than the gaps between their gill raker 'mesh'.

The linear speeds of the vortices in all three preserved paddlefish were very similar ($p = 0.06$) (Table 4), demonstrating that the flow speeds within the vortices were comparable in different individuals. However, the vortices traveled at significantly ($p < 0.0001$) different revolutions per minute ($p < 0.0001$) and had different speeds along the axis of travel ($p = 0.0005$). Additionally, the diameter of the vortex impacts the linear speed. Since linear speed is the angular speed multiplied by the radius of the vortex, a vortex with a larger radius would have a higher linear speed compared to a vortex with the same angular speed but smaller radius. Vortices with the same radius but different angular speeds would also have varying linear speeds. A higher angular speed would mean a higher

linear speed, and therefore a faster vortex. The medium and large paddlefish vortices had similar diameters ($p = 0.06$), and similar linear speeds ($p = 0.06$), therefore their angular speeds must not vary substantially.

While the vortices had similar linear speeds, they had significantly different speeds when only considering the axial distance traveled down the arch ($p = 0.0005$). These differences may be because the arches were at different angles with respect to the oncoming water. They may also be due to the size of the paddlefish and the height of the branchial arch. Another factor to consider is the placement of the infusion needle in the arch. For each paddlefish, the needle was inserted according to the clearest vortices visible from that insertion spot. Therefore, the placement of the needle was slightly different for each paddlefish. This caused a different layer of the cylindrical vortex behind the arch to be dyed in each paddlefish.

The vortices in the paddlefish oral cavity and the 3D models are fed continuously from the influx of water into the gape, which provides a sustained high-speed flow to the outermost layers of each vortex. Water flows over the top of each arch continuously during feeding, providing the flow that the vortex needs to keep spinning. Sanderson et al. (2016) analyzed the vortices within 3D models with 90° ribs. These vortices were in the outermost layer of water of the vortex, the layer closest to the incoming flow of water. This layer has a high shear rate, and the water in this outer layer is constantly scouring the mesh and exiting from the vortex. The vortices analyzed in this thesis were closer to the center of the vortex, and had a small diameter relative to the vortices analyzed in Sanderson et al. (2016). The 90° model vortices in this thesis had an average diameter of 0.09 cm, while the 90° model vortices in Sanderson et al. (2016) had an average diameter of 0.30 cm. The

vortices in the 90° model from Sanderson et al. (2016) had a linear speed of 9.7 cm s⁻¹, while the vortices analyzed in this thesis from the 90° model had a much slower average linear speed of 2.99 cm s⁻¹. However, both sets of vortices had the same average rotational speed, 626 revolutions min⁻¹, and the same speed along their axis in the gill slit, 3.0 cm s⁻¹. This demonstrates that, for the vortices in the 90° model, rotational speed is not dependent on the diameter of the vortex while linear speed is dependent on the diameter. These data are indicative of a forced vortex, which would have faster linear speeds in the outer layers and slower linear speeds in the inner layers (Rousseaux et al., 2001).

Using the three types of 3D models, which were identical except for the differences in arch angles, we were able to analyze the effects of changing arch angle on the vortices. The main effect that the change in arch angle had on the vortices was that an increased angle was associated with an increased rotational speed in the 110° model ($p < 0.0001$) and an increased diameter in the 55° model ($p < 0.0001$, Table 5). The water in the flow tank was consistent in speed during all experiments. The change in rotational speed in the 110° model may be caused by the change in arch angle. However, since the 90° and 55° models did not have significantly different rotational speeds, the difference in the 110° may not be related to arch angle. Instead, the difference could be due to the slant of the wall on the inside of the gill slit. The vertical wall of the step is not completely vertical inside the 110° model, but slanted, which may change the qualities of the vortex within the slit.

Two of the three vortices, the vortices in the 90° and 110° models, had similar diameters but different rotational speeds. The 55° model had a substantially larger vortex diameter ($p < 0.0001$). Since paddlefish branchial arch angles decrease successively toward the back of the mouth, a change in arch angle could potentially impact vortex diameter,

rotational speed, and linear speed. In turn, these variables could influence particle transport by the vortices. Future experiments could study vortices behind the gill arches farther back in the paddlefish mouth. Since these gill arches have different angles than the arches studied in this experiment, it would be interesting to see how the vortex features differ between the arches. Particles could also be used in these experiments to see how efficiently each vortex is able to retain and transport particles. Since all of the arches in the paddlefish mouth have gill rakers (Rosen and Hales, 1981), each arch must play an important role in particle capture. However, the arches may not have equal roles, and some may be more important than others.

These findings are unexpected when seen in light of the data found in previous publications. Using computational fluid dynamics, another study found that volume flow rate from the gill slits in a simulated conical model decreased when the angle of the arch increased from 55° to 90° (Cheer et al., 2001). However, that study did not take into account the formation of vortices inside the gill slits. Therefore, it is possible that when vortices are present, the flow of water through the slits decreases. Additionally, the same study found that volume flow rate decreased in the slits with each successive arch moving to the posterior of the model. This could have implications for the vortices behind arches further posterior in the models. It is possible that the vortices slow down behind successive arches. This would lead to lower linear speed and rotational speed in each vortex. The diameters of the vortices might also change, especially since the width of each gill slit varies. As the width of the gill slit decreases, the vortex has less potential space to occupy, and might therefore become smaller in diameter. Additionally, this thesis demonstrated that the vortices behind arches with varying angles differ.

Future studies could analyze the differences of vortex speed between different sets of arches in the same model. The formation of these vortices would change the speed of flow inside the gill slits, as well as the speed of the water as it exits from each gill slit. There could possibly be an angle at which the vortex no longer forms. This angle would have to be acute and almost parallel to the water flow as it enters the paddlefish mouth. To study this, more models could be made with small angles, and their ability to retain and transport particles could be studied. The changing angle of the arches changes, in turn, the angle of the gill rakers with respect to the incoming water. When the angle of the oncoming water at the surface of the gill rakers changed from 75° to 60° in computational fluid dynamics studies (Cheer et al., 2012), the speed of the water passing between the gill rakers increased. Reducing the angle also causes the gaps between gill rakes to be more leaky, letting more water escape (Cheer et al., 2012). Therefore, changing the angle of the gill arches has an effect on not only the vortices behind those arches, but also affects the flow on the gill rakers at the lateral edge of the arches. A different computational fluid dynamics model could be created taking into account the findings of this study. This model could study the effects of changing arch angle on the vortices behind those arches. It could also study the effects of a vortex flow on the gill rakers ventral to that flow. Specifically, a future study could look at how and where water escapes between the gill rakers, and also study the impact of a vortex flow on the vortices between gill rakers. This would help expand the knowledge on how the larger vortices impact water flow at the level of the gill rakers.

The vortices quantified in the paddlefish had linear speeds closest to the vortices in the 55° 3D model, and rotational speeds closest to the 55° and 90° models (Table 4 and Table 5). The diameters of the vortices in the paddlefish were similar to the diameter of the

55° model vortices, and larger than the vortices in the other two models. Since linear speed is dependent on diameter, the similarity between the 55° model vortices and the paddlefish vortices may have more to do with the similarity in diameter than similarity between arch angles. The calculation of rotational speed is independent of diameter, and therefore the similarities between the paddlefish vortices and the 55° and 90° models are notable. The values quantified from the 110° model were the least similar to the values from the paddlefish. Since the paddlefish have arch angles closer to 55°, this makes sense. However, there could be other qualities of the paddlefish mouth influencing the vortices and causing them to differ from the model values. The paddlefish mouth is more bowl-shaped than the conical 3D models. Additionally, the branchial arches are much thinner than the ribs in the 3D models. There are also physical differences between the ribs on the 3D models and paddlefish gill arches. Before the gill arch meets the basibranchial, there is a sharp, almost 90° turn in the arch, creating a small space with an irregular flow pattern. This shape is not modeled in the 3D models for this study. Further studies could create a 3D model that more closely matches a paddlefish mouth. Information from this thesis, such as the arch angles, gill slit area, and open gape area, could be used to help create the 3D model.

Area of paddlefish gill slits and open gape

We predicted that the total open area of the gill slits would be greater than the area of the open gape so that water entering the mouth would not meet with resistance from water not able to exit the oral cavity. The results confirm this hypothesis: the area of the gill slits is even at times greater than twice the area of the open gape (Table 2). During ram ventilation, this ratio will allow water to exit the oral cavity easily. When paddlefish switch

from ram ventilation to filter feeding, their buccal flow velocities increase (Sanderson et al., 1994). This indicates that there is an even greater need for water to escape during ram suspension feeding to avoid resistance. However, our results do not take into account the gill rakers, which will partially block the gill slits during feeding. Paddlefish move their gill rakers so that they are at a 60° angle from the gill arch (Imms, 1904). Future experiments could attempt to model this gill raker angle, and more accurately match the inside of the paddlefish mouth. In previous experiments, a micro-thermistor flow probe has been inserted into the oral cavity of paddlefish to record flow velocities inside the mouth (Sanderson et al., 1994). A similar method could be used to insert an endoscope into the oral cavity of live paddlefish, as was done with tilapia (Smith and Sanderson, 2007). This would allow the feeding process to be studied in live paddlefish, and direct observation of particle movement.

Degree of paddlefish yaw

As a paddlefish swims, it yaws back and forth in the water. A recent study has shown that this undulation can optimize propulsion, respiration, and flow sensing in many fish (Akanyeti et al., 2016). This movement may also help fish during feeding. When a fish yaws, it changes the angle of the water with respect to the gill arch. Even a slight angle change can have a large impact on shape and speed of the vortex behind the gill arch. When filming the vortices within the paddlefish mouth, the vortices became clearer and easier to follow when the paddlefish was rotated slightly to the right. The paddlefish may be using this movement to stir up particles within its mouth, clear its gill rakers, or change the flow pattern in some way. Future studies should research the exact impact of this yaw

movement on the vortices within the paddlefish mouth. Studying yaw would help in the understanding of how paddlefish suspension feeding works in real life situations, when water is flowing turbulently.

Tables and Figures

Table 1. Paddlefish branchial arch angles

Location	Angle (degrees)
	mean \pm s.d. (n = 3)
Roof	46.4 \pm 5.4
Epibranchial 1	41.4 \pm 4.5
Epibranchial 2	35.4 \pm 5.0
Epibranchial 3	33.9 \pm 4.6
Epibranchial 4	18.3 \pm 7.1
Lower Jaw	41.9 \pm 4.0
Ceratobranchial 1	26.1 \pm 2.6
Ceratobranchial 2	20.7 \pm 3.3
Ceratobranchial 3	18.8 \pm 5.0
Ceratobranchial 4	15.0 \pm 5.0

Table 2. Paddlefish gill slit area and open gape area

Location	Area (cm ²)		
	Small Paddlefish	Medium Paddlefish	Large Paddlefish
Gill Slit 1	6.4	5.0	11.1
Gill Slit 2	4.3	5.0	8.4
Gill Slit 3	3.4	3.3	5.6
Gill Slit 4	2.5	1.8	5.1
Gill Slit 5	0.5	0.6	1.3
Gill Slit Total	17.0	15.7	31.5
Gape	9.0	11.1	12.0
Ratio of gill slit area to open gape	1.89	1.45	4.37

Table 3: Aspect ratio of paddlefish branchial arches.

Paddlefish	Width (cm)	Height (cm)	Aspect Ratio
Small	0.37	0.38	0.97
Medium	0.48	0.45	1.06
Large	0.79	0.50	1.58

Table 4. Parameters quantified for recirculation region of paddlefish preserved in suspension-feeding position (mean \pm s.d., n = 5).

Paddlefish Specimen	Diameter (cm)	Linear Speed (cm s ⁻¹)	Rotational Speed (revolutions min ⁻¹)	Speed along axis in gill slit (cm s ⁻¹)
Small	0.19 \pm 0.03	6.4 \pm 1.4	641.4 \pm 42.1	5.1 \pm 0.3
Medium	0.26 \pm 0.06	5.5 \pm 1.5	398.7 \pm 39.5	4.1 \pm 0.8
Large	0.23 \pm 0.02	4.3 \pm 0.7	359.4 \pm 26.2	6.3 \pm 0.5
Mean \pm s.e.	0.23 \pm 0.04	5.4 \pm 1.1	466.5 \pm 152.7	5.2 \pm 1.1

Table 5: Parameters quantified for recirculation region of 3D models (mean \pm s.d., n = 5).

Angle of Model	Diameter (cm)	Linear Speed (cm s ⁻¹)	Rotational Speed (revolutions min ⁻¹)	Speed along axis in gill slit (cm s ⁻¹)
90°	0.09 \pm 0.02	2.9 \pm 0.8	626.4 \pm 68.1	3.0 \pm 0.4
55°	0.21 \pm 0.02	5.8 \pm 0.7	535.8 \pm 51.7	3.3 \pm 0.1
110°	0.09 \pm 0.00	4.5 \pm 0.7	943.4 \pm 149.0	3.8 \pm 0.2

Table 6: Flow speed experiments (mean \pm s.d., n = 3).

Paddlefish	3 cm anterior of rostrum (cm s ⁻¹)	Flow Speeds	
		Directly anterior to gape at height of first ceratobranchial (cm s ⁻¹)	Directly dorsal to first ceratobranchial (cm s ⁻¹)
Small	13.2 \pm 0.4	11.8 \pm 0.2	11.1 \pm 0.3
Medium	12.4 \pm 0.2	10.5 \pm 0.3	10.2 \pm 0.1
Large	12.4 \pm 0.3	9.7 \pm 0.3	7.9 \pm 0.2

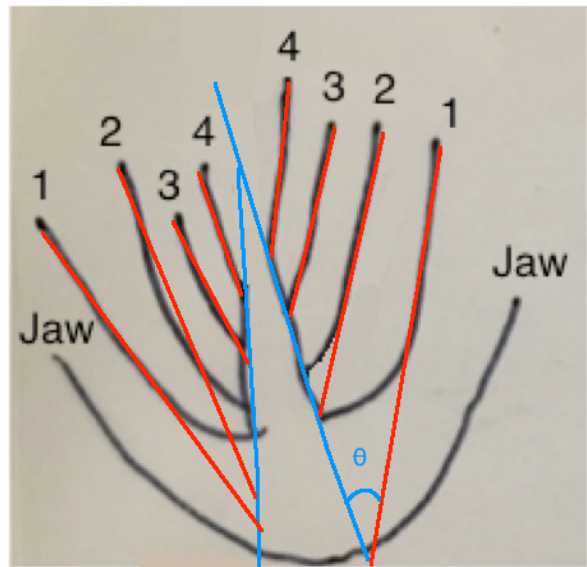
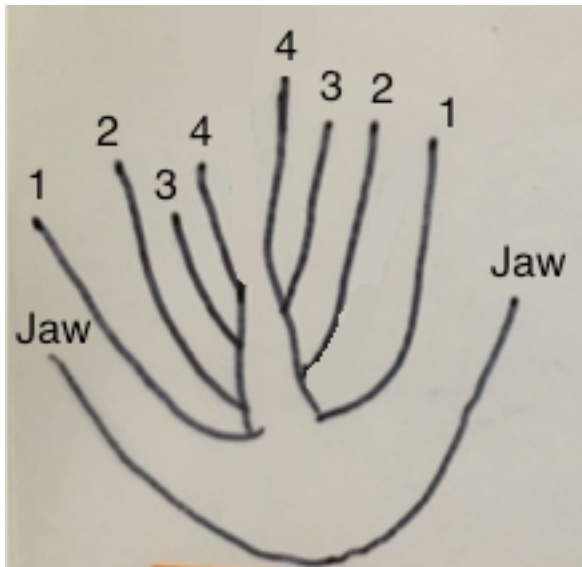


Figure 1. Tracing of the floor of the paddlefish oral cavity. On the right, the angle at which each epibranchial or ceratobranchial intersected the center "V" of the oral cavity has been traced. Numbers refer to ceratobranchials, decreasing successively in angle towards the posterior.

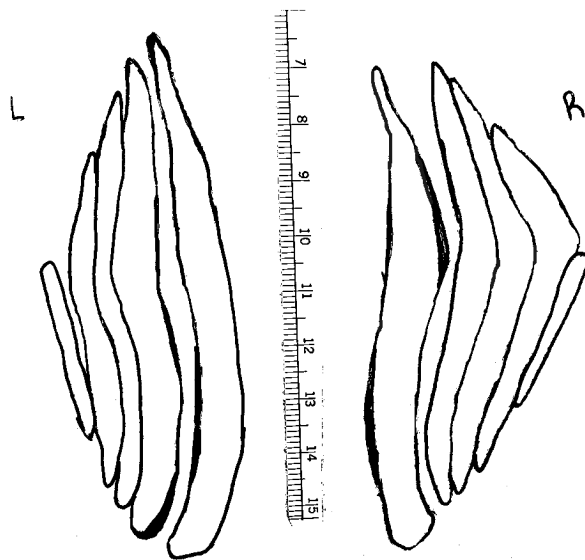


Figure 2. Tracing of the large paddlefish gill slits. The right side (R) is the right side of the paddlefish and the left side (L) is the left side of the paddlefish. Scale in centimeters is in the middle.



Figure 3. View down the rostrum into the paddlefish mouth (small paddlefish). Scale in centimeters is on the right. Steel mesh covering the gill slit behind the first ceratobranchial on the paddlefish's left side is visible.

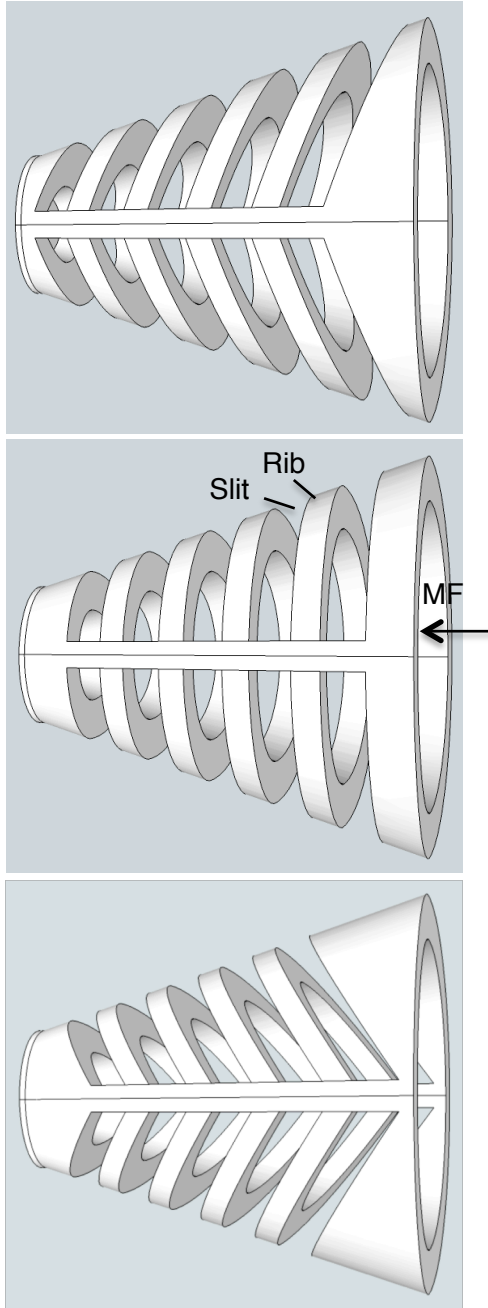


Figure 4. Computer aided design of the 3D models as viewed from above. Mainstream flow (MF) enters from the right and exits through the slits. The top model is 110°, the middle model is 90°, and the bottom model is 55°. (Modified from Sanderson et al., 2016).



Figure 5. Vortices behind the first ceratobranchial in the three paddlefish. The top photograph is the small paddlefish, the middle photograph is the medium paddlefish, and the bottom photograph is the large paddlefish. Flow enters from the right.

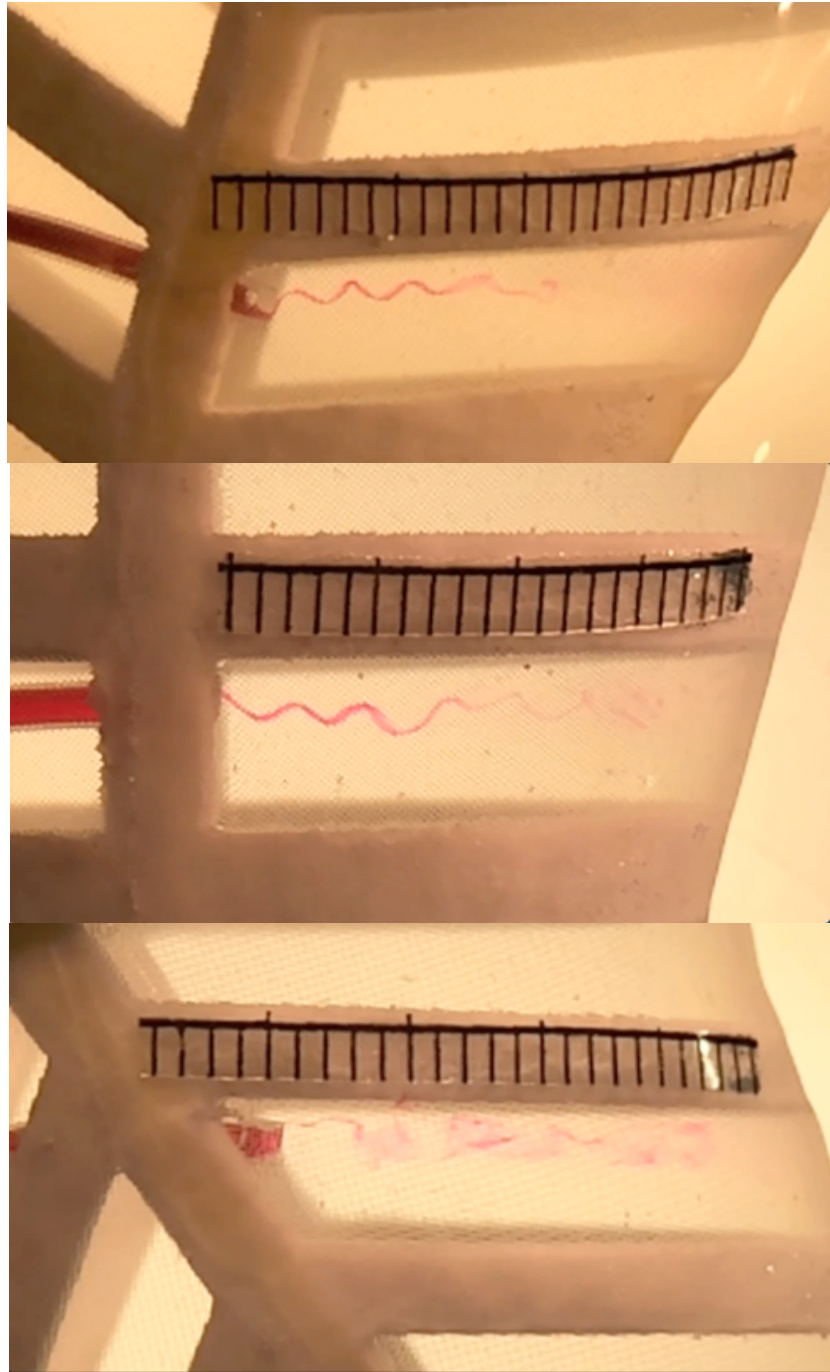


Figure 6. Vortices inside the three 3D models as shown from above with a millimeter scale. The top model is 110° , the middle model is 90° , and the bottom model is 55° . Flow entering parallel to the solid midline, and vortex traveling from the left to right in the photograph.

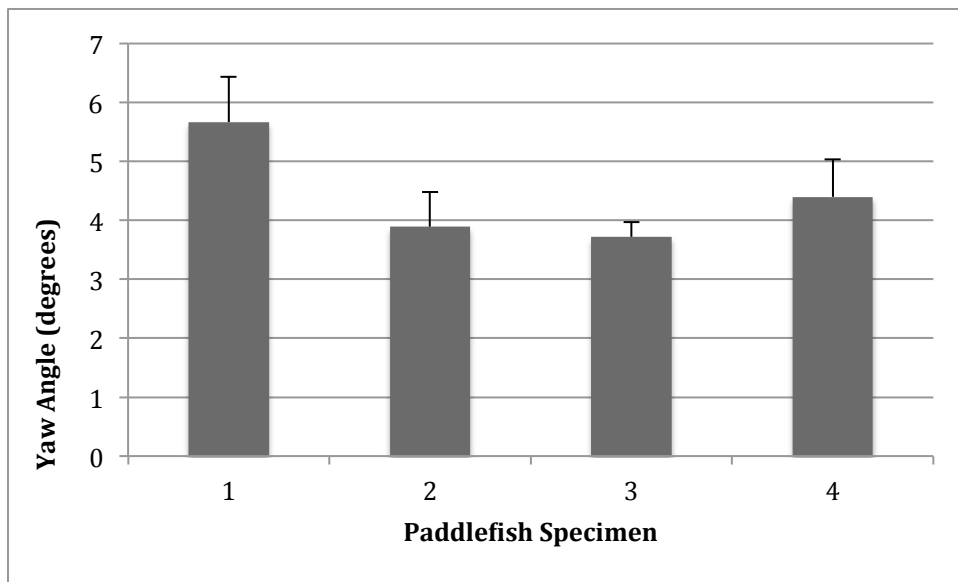


Figure 7. Paddlefish yaw angles (mean \pm s.e.).

References

- Akanyeti, O., Thornycroft, P.J.M., Lauder, G.V., Yanagitsuru, Y.R., Peterson, A.N., Liao, J.C. (2016) Fish optimize sensing and respiration during undulatory swimming. *Nat. Commun.* 7: 11044.
- Bemis, W.E., Findeis, E.K., Grande, L. (1997) An overview of acipenseriformes. *Environmental Biology of Fishes.* 48: 25 – 71.
- Brainerd, E.L. (2001) Caught in the crossflow. *Nature*, 412: 387-388.
- Burggren, W. W., Bemis, W. E. (1992) Metabolism and ram gill ventilation in juvenile paddlefish, *Polyodon spathula* (Chondrostei: Polyodontidae). *Physiol. Zool.* 65: 515–539.
- Callan, W.T., Sanderson, S.L. (2003) Feeding mechanisms in carp: crossflow filtration, palatal protrusions and flow reversals. *J. Exp. Biol.* 206: 883 – 892.
- Cheer, A. Y., Cheung, S., Hung, T.C., Piedrahita, R.H., Sanderson, S.L. (2012) Computational fluid dynamics of fish gill rakers during crossflow filtration. *Bull. Math. Biol.* 74: 981 – 1000.
- Cheer, A.Y., Ogami, Y., Sanderson, S.L. (2001) Computational fluid dynamics in the oral cavity of ram suspension-feeding fishes. *J. Theor. Biol.* 210: 463 – 474.
- Drenner, R.W., Hambright, K.D., Vinyard, G.L., Gophen, M., Pollinger, U. (1987) Experimental study of size-selective phytoplankton grazing by filter-feeding cichlid and the cichlid's effects on plankton community structure. *American Society of Limnology and Oceanography.* 32: 1138-1144.
- Drenner, R.W., Taylor, S.B., Lazzaro, X., Kettle, D. (1984) Particle-grazing and plankton community impact of an omnivorous cichlid. *Transactions of the American Fisheries Society* 113: 397 – 402.
- Friedland, K.D. (1985) Functional morphology of the branchial basket structures associated with feeding in the Atlantic menhaden, *Brevoortia tyrannus* (Pisces: Clupeidae). *American Society of Ichthyologists and Herpetologists.* 1985: 1018 – 1027.
- Grady, J. (2004) *Polyodon spathula*. The IUCN Red List of Threatened Species. www.iucnredlist.org. Downloaded on 13 April 2016.
- Grande, L., Bemis, W.E. (1991) Osteology and phylogenetic relationships of fossil and recent paddlefishes (Polyodontidae) with comments on the interrelationships of acipenseriformes. *Memoir (Society of Vertebrate Paleontology).* 1: 1 – 121.

- Greenwood, P.E., Ward, L.M., Russell, D.F., Neiman, A.B., Moss, F. (2000) Stochastic resonance enhances the electrosensory information available to paddlefish for prey capture. *Physical Review Letters*. 84: 4773-4776.
- Imms, A. D. (1904) Notes on the gill-rakers of the spoonbill sturgeon, *Polyodon spathula*. *P. Zool. Soc. Lond* 2: 22-35.
- Jaffrin, M. Y. (2012) Hydrodynamic techniques to enhance membrane filtration. *Annu. Rev. Fluid Mech.* 44: 77-96.
- Jennings, C.A., Zigler, S.J. (2009) Biology and life history of paddlefish in North America: an update. *American Fisheries Society Symposium*. 66: 1 - 22.
- LaBarbera, M., Vogel, S. (1976) An inexpensive thermistor flowmeter for aquatic biology. *Limnol. Oceanogr.* 21: 750-756.
- Lu, M., Xie, P. (2001) Impacts of filter-feeding fishes on the long-term changes of crustacean zooplankton in a eutrophic subtropical Chinese lake. *Journal of Freshwater Ecology* 16: 219 - 228.
- Motta, P. J., Maslanka, M., Hueter, R.E., Davis, R.L., de la Parra, R., Mulvany, S.L., Habegger, M.L., Strother, J.A., Mara, K.R., Gardiner, J.M., Tyminski, J.P., Zeigler, L.D. (2010) Feeding anatomy, filter-feeding rate, and diet of whale sharks *Rhincodon typus* during surface ram filter feeding off the Yucatan Peninsula, Mexico. *Zoology*. 113: 199-212.
- Paig-Tran, E.W., Bizzarro, J.J., Strother, J.A., Summers, A.P. (2011) Bottles as models: predicting the effects of varying swimming speed and morphology on size selectivity and filtering efficiency in fishes. *J. Exp. Biol.* 214: 1643 - 1654.
- Paig-Tran, E.W., Kleinteich, T., Summers, A.P. (2013) The filter pads and filtration mechanisms of the devil rays: variation at macro and microscopic scales. *Journal of Morphology*. 274: 1026 - 1043.
- Rosen, R.A., Hales, D.C. (1981) Feeding of paddlefish, *Polyodon spathula*. *American Society of Ichthyologists and Herpetologists*. 1981: 441 - 455.
- Rousseaux, J.M., Muhr, H., Plasari, E. (2001). Mixing and micromixing times in the forced vortex region of unbaffled mixing devices. *The Canadian Journal of Chemical Engineering*. 79: 697 - 707.
- Sanderson, S.L., Cheer, A.Y., Goodrich, J.S., Graziano, J.D., Callan, T. (2001) Crossflow filtration in suspension-feeding fishes. *Nature*. 412: 439 - 441.
- Sanderson, S.L., Cech, J.J., Cheer, A.Y. (1994) Paddlefish buccal flow velocity during ram suspension-feeding and ram ventilation. *J. Exp. Biol.* 186: 145 - 156.

- Sanderson, S.L., Roberts, E., Lineburg, J., Brooks, H. (2016) Fish mouths as engineering structures for vortical cross-step filtration. *Nature Communications*. 7: 11092.
- Sanderson, S.L., Stebar, M.C., Ackermann, K.L., Jones, S.H., Batjakas I.E., Kaufman, L. (1996) Mucus entrapment of particles by a suspension-feeding tilapia (Pisces: Cichlidae). *J. Exp. Biol.* 199: 1743 – 1756.
- Sims, D. W. (2008) Sieving a living: a review of the biology, ecology and conservation status of the plankton-feeding basking shark *Cetorhinus maximus*. *Adv. Mar. Biol.* 54: 171–220.
- Smith, J.C., Sanderson, S.L. (2007) Mucus function and crossflow filtration in a fish with gill rakers removed versus intact. *J. Exp. Biol.* 210: 2706 – 2713.
- Smith, J. C., Sanderson, S. L. (2008) Intra-oral flow patterns and speeds in a suspension-feeding fish with gill rakers removed versus intact. *Biol. Bull.* 215: 309–318.
- Smith, J.C., Sanderson, S.L. (2013) Particle retention in suspension-feeding fish after removal of filtration structures. *Zoology*. 116: 348 – 355.
- Torres, G.S., Silva, L.H.S., Rangel, L.M., Attayde, J.L., Huszar, V.L.M. (2016) Cyanobacteria are controlled by omnivorous filter-feeding fish (Nile tilapia) in a tropical eutrophic reservoir. *Hydrobiologia*. 765: 115 – 129.
- Wilkins, L.A., Russell, D.F., Pei, X., Gurgens, C. (1997) The Paddlefish Rostrum Functions as an Electrosensory Antenna in Plankton Feeding. *Proceedings: Biological Sciences*. 264: 1723 - 1729.
- Wojtenek, W., Pei, X., Wilkins, L.A. (2001) Paddlefish Strike at Artificial Dipoles Simulating the Weak Electrical Fields of Planktonic Prey. *The Journal of Experimental Biology*. 204: 1391–1399.
- Zhu, Y.J., Li, X.M., Yang, D.G. (2014) Food preference of paddlefish, *Polyodon spathula* (Walbaum, 1792), in polyculture with bighead carp *Aristichthys nobilis* (Richardson, 1845) in non-fed ponds. *Journal of Applied Ichthyology*. 30: 1596–160.